The Gemini Planet Imager Calibration Testbed

J. Kent Wallace*[a], Rick Burruss[a], Laurent Pueyo[a], Remi Soummer[b], Chris Shelton[a], Randall Bartos[a], Felipe Fregoso[a], Bijan Nemati[a], Paul Best[a] , John Angione[a]

[a]Jet Propulsion Laboratory, California Institute of Technology, 4800 Oak Grove Dr., Pasadena, CA, USA 91109;
[b]Space Telescope Science Institute, 3700 San Martin Drive, Baltimore, MD USA 21218

ABSTRACT

The calibration wavefront system for GPI will measure the complex wavefront at the apodized pupil and provide slow phase corrections to the AO system to mitigate against errors that would cause a loss in contrast. This talk describes both the low-order and high-order sensors in the calibration wavefront sensor and how the information is combined to form the wavefront estimate before the coronagraph. Expected performance for this wavefront sensor will also be described for typical observing scenarios. Finally, we will show labratory results from our calibration testbed that demonstrate the instrument performance at levels commensurate with those required on the GPI instrument.

Keywords: interferometry, wavefront sensing, coronagraphy, planet detection

1. INTRODUCTION

The Gemini Planet Imager will employ an apodized-pupil coronagraph to make direct detections of faint companions of nearby stars to a contrast level of the 10-7 within a few lambda/D of the parent star. Such high contrasts from the ground require exquisite wavefront sensing and control both for the AO system as well as for the coronagraph. Un-sensed non-common path phase and amplitude errors after the wavefront sensor dichroic but before the coronagraph would lead to speckles which would ultimately limit the contrast. The calibration wavefront system for GPI will measure the complex wavefront at the system pupil before the apodizer and provide slow phase corrections to the AO system to mitigate errors that would cause a loss in contrast.

Non-common path wave front errors, it not sensed and corrected, will set the limit for achievable contrast for a ground based AO system. These errors are particularly vexing due to their temporal evolution. If they were perfectly static, they could be measured once and subsequently removed in post processing. If they were perfectly random, they would average out to a smooth floor over long integrations. Non-common path errors that limit contrast tend to evolve over times scales of a few minutes to 10's of minutes and therefore must be sensed and corrected during a science observation. The main goal of the calibration system for GPI is to sense these wave front errors and provide a measurement to the AO system so that they may be corrected. The most crucial wave front errors are those at spatial frequencies corresponding to the "dark hole" region of the PSF and outside the coronagraph's inner working distance – 4-22 cycles per pupil. The calibration subsystem that will measure these mid-spatial frequency errors is called the high-order wave front sensor, HOWFS.

Many coronagraphs, including the apodized pupil Lyot coronagraph (APLC[3]) employed by GPI, are very sensitive to the location of the star on the focal plane mask – centering errors of as little as 3 miliarcseconds can begin to degrade contrast. As a separate task the calibration system will employ a low-order wave front sensor to establish the boresite of the instrument and ensure the centering is sufficient for achieving and maintaining high-contrast. This boresite will also be accurate and stable for precision astrometry. This calibration element is known as the low-order wave front sensor, or LOWFS, and will also measure the low-spatial-frequency wave front errors (e.g. focus) that the HOWFS is blind to.

*James.K.Wallace@jpl.nasa.gov; phone 1 818 393-7066; jpl.nasa.gov

A description of the calibration subsystem is most easily accomplished by following the starlight path when encountering it. The system level drawing (Figure 1) will aide in this discussion. The light after leaving the apodized pupil converges to the focal plane to form an image at the focal plane mask. The light falling within the hard-edged focal plane mask will compose the reference arm, the light reflected will form the science arm, and the light that goes down both arms will meet again at the re-combination beamsplitter and be sensed at the HOWFS. The following discussion will then be in the same order: reference arm, science arm and HOWFS arm.
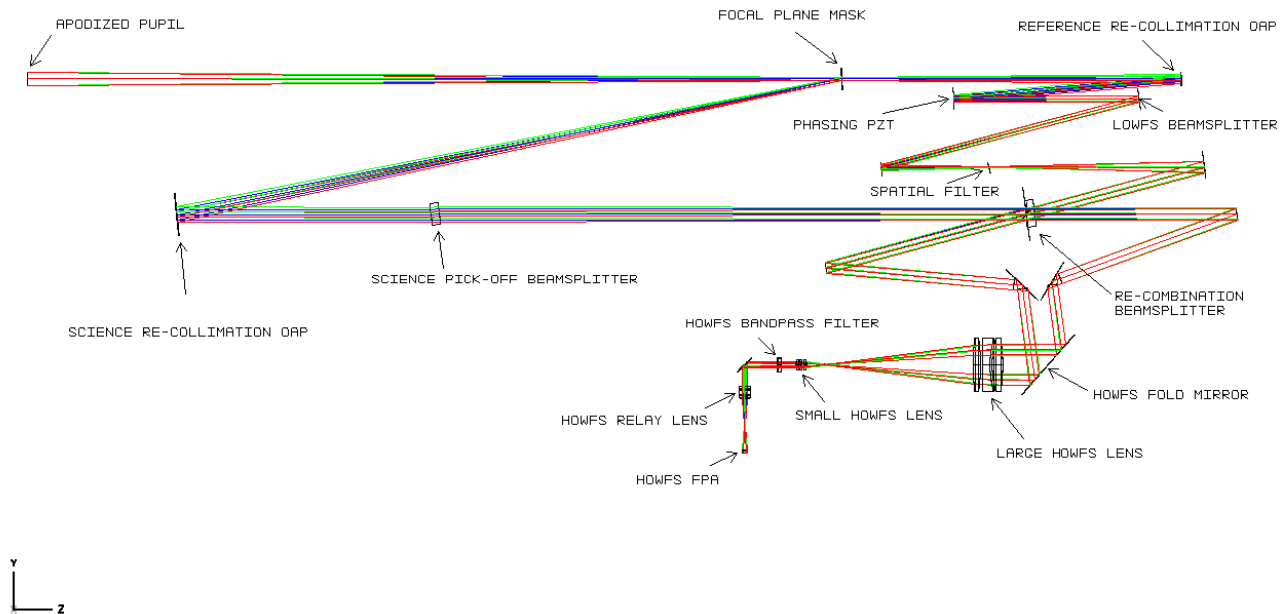

Fig. 1. Optical layout of the GPI calibration system. Light from the adaptive optics system enters from the top left, passes through the apodized pupil to the focal plane that is located in the top-center of the drawing. The majority of the starlight passes through the focal plane mask and into the reference arm in the upper right of the diagram. Light that reflects off the focal plane mask heads to the science path in the lower left of the diagram. Both beams meet a the science re-combination beamsplitter and are sensed on the high-order wavefront sensor in the lower right portion of the image.

1.1 Cal System Optical Design

The calibration subsystem consists of two primary sub-elements: the high-order wave front sensor (HOWFS), the low order wave front sensor (LOWFS). This section will offer a description of the relevant parts of each sub-element, a description of the driving optical concerns and a ray trace of the sub-element. After a discussion of the optical design, we will review the simulation and predicted performance of the system.

1.2 Reference Arm

The starting point for the reference arm is the focal plane mask, or more specifically, the hole in the center of the focal plane mask. Several different focal plane masks are available in the focal plane mask occultor mechanism. The masks will be provided by our collaborators at AMNH while the mechanism is the responsibility of JPL. After the focal plane mask, the next optic is the reference arm recollimation OAP. This optic creates a five millimeter diameter beam. Next, the beam strikes the Tip/Tilt/Piston PZT mirror. This mirror plays several roles: 1) phase shifting for the high-order wave front sensor and 2) pointing correction for the pinhole spatial filter. The phase shifting is done in a collimated beam and all points in the pupil are shifted in phase equally

After the phase shifting mirror, the beam either passes through the beamsplitter to the LOWFS or reflects to the pinhole spatial filter. The LOWFS will be described below, so lets follow the path to the spatial filter assembly. This is the

assembly that serves to remove residual wavefront errors on the beam such that the phase and amplitude of the reference beam electric field at recombination is largely uniform. The first OAP of the assembly forms a focus at the pinhole (currently sized to 1.4 λ/D, diameter, at 1.635 μm). The spatially filtered light passing through this pinhole is re-collimated by the second OAP in the assembly to roughly ten millimeters in diameter. Centering of the light on the pinhole is crucial for consistent, repeatable performance for the HOWFS. However, sensing where this beam is when it is even a little off from the pinhole is a challenge. To expedite the acquisition we have implemented what we call the pinhole camera which allows us to directly measure the starlight relative to the pinhole and thus expedite the co-alignment. Finally, we have a shutter in the reference arm that allows us to block the light. This option is necessary for allowing us to measure the transmission function of the input pupil apodizer and establishing detector darks without affecting the operation of the rest of the instrument.

1.3 Science Arm

For the science beam, the starlight suppression has just occurred at the focal plane mask, and the science re-collimation OAP creates a beam that is ten millimeters in diameter and parallel to the beam incoming to the focal plane mask (offset by 128 millimeters). A small portion of this light (roughly 20%, broadband) will pass through a spectrally-neutral, broadband beam splitter. This light will then pass through the science arm shutter (if it is open) and on to the recombination beamsplitter. The light that gets reflected from the science pick-off beam splitter heads to the pointing-and-centering mirror pair that feed the Integral Field Spectrograph (IFS). This mirror pair ensures proper image-plane and pupil-plane alignment between the calibration sub-system and the IFS.

1.4 High-order wavefront sensing arm

As mentioned previously, the optical layout of the HOWFS sub-element will begin at the location of the re-imaged pupil which occurs after the beams have been re-combined. This pupil is formed very near to vertex of the merge prism. Now, there are some optical matters that need to be addressed before the re-combination beamsplitter, and this is because the calibration HOWFS is a broad-band, white-light, phase-shifting interferometer. For the interferometer to perform properly, its internal optical paths, as a function of wavelength, from the point of separation at the focal-plane mask to the point of recombination must match to within a small fraction of a micron. This puts a constraint on the allowable dispersion (differential glass thickness) and DC phasing between the two arms of the interferometer. An interferometer is also sensitive to internal optical pathlength disturbances. In our case, these pathlength vibrations are only problematic when they are near the demodulation frequency. If they are at a higher frequency, they will average out during the integration time of a single measurement, while if they are slower, they will be frozen out. We have designed the optical beam height (and mechanical mounts) from the mounting surface to be small so as to increase any mount-related resonant frequency.

Since we're working on a broadband astronomical instrument, atmospheric refraction is of necessity a concern. Left uncorrected, the residual atmospheric refraction will produce a chromatic smearing in the image plane and chromatic shear in the pupil plane. Both of these would have detrimental effects on the performance of both the LOWFS and HOWFS. An Atmospheric Despersion Corrector has been added to mitigate against these effects. All of these optical aspects have been addressed before the HOWFS relay.
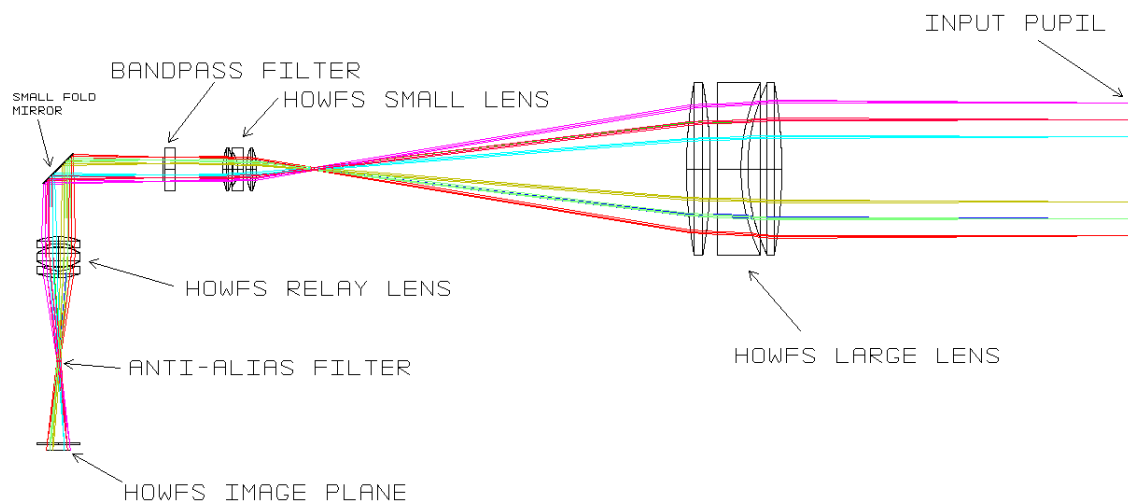
Fig. 2. Layout of high-order wavefront sensing arm of the calibration system. Two pupils, one each from the front and back of the re-combination beamsplitter are imaged at the plane in the upper-right of the drawing. The big lens images these pupils to infinity while forming an image in the focal plane. A re-collimation lens forms demagnified pupil images at its focus. A one-to-one lens relays this image to the final image plane.

The layout of the HOWFS optical relay is shown above in Figure 2. The pupil is traced from the upper right. The pupil size is ten millimeters in diameter and the separation is designed such that upon demagnification, the two pupil images are on separate readout quadrants of the InGaAs array. The HOWFS fold mirror redirects the light to the HOWFS pupil lens. This lens is designed such that the input pupil is located at the back focal length so it is imaged to infinity. At the front focus of this lens is located the anti-aliasing spatial filter. The HOWFS pupil lens is a triplet designed to give good, broadband imaging from 0.9 μm – 2.4 μm. The lens materials are common for the visible/near-infrared and the lens surface shapes are plano-spherical.

The next optical element is the pupil re-imaging lens. It is also a triplet based upon the design of the HOWFS pupil lens. In the space before this lens, the pupil is at infinity, so after this lens it is re-imaged to the back focal length and de-magnified to the size and separation that will occur on the final image plane. This pupil image is formed near the location of the warm chromatic filter this is advantageous as it makes the final image location of the focal plane array insensitive to the wedges in the warm chromatic filter.

1.5 Low-order wavefront sensor arm

In the reference arm of the calibration system, a real pupil image is formed approximately 75 millimeters after the LOWFS pick-off beamsplitter. The optical layout for the LOWFS, a traditional Shack-Hartman, is shown in Figure 3 below:

LOWFS IMAGE PLANE

LOWFS RELAY LENS 2

LOWFS RELAY LENS 1

FOCAL PLANE MASK

REFERENCE OAP

Y

Z

PHASING MIRROR
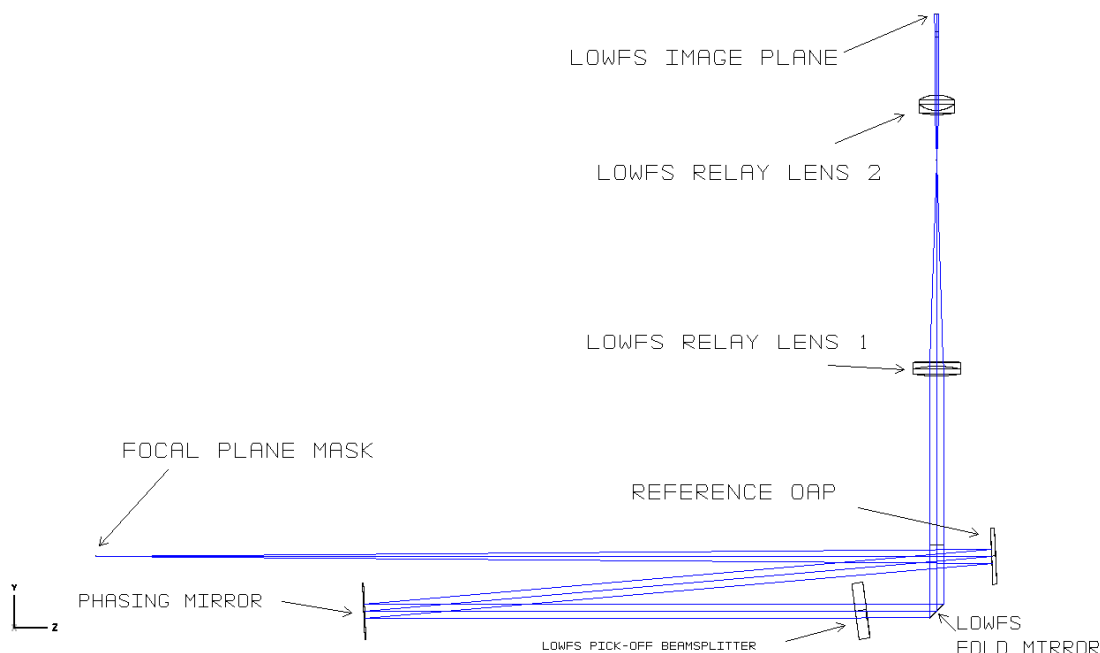
LOWFS PICK-OFF BEAMSPLITTER

LOWFS
FOLD MIRROR

Fig. 3. Optical layout of the low-order wavefront sensor or LOWFS. This image shows the light leaving the center of the focal plane mask on the left. This light is re-collimated, reflects off the phase-shifting mirror, through a beamsplitter where the pupil is re-imaged. This pupil is relayed to form a real image on the lenslets. The lenslet array is just before the InGaAs array.

The two lenses are off-the-shelf and serve to compress the beam to the appropriate size for the lenslet array. The lenslet is also off-the-shelf and samples the pupil with an array of 7x7 subapertuers. These spots are then imaged directly onto the final Shack-Hartmann sensor. A geometrical optics analysis of this wave front sensor is only useful to get pupil locations and sizes correct. The sensor works by measuring tilts in diffraction PSF's and has been modelled extensively and this work is described in the performance simulation section.

2. CALIBRATION TESTBED RESULTS

In order to test the principles of calibration wave front sensing, we have constructed a testbed. This testbed has source optics which have a pupil and image plane conjugates that map directly to those that will be on the GPI instrument. The testbed system itself is a fully functional duplicate of the final GPI calibration system with both a HOWFS and a LOWFS. We will use this testbed to demonstrate algorithms and performance for wave front control at levels consistent with those for the final GPI calibration system. We will also be able to explore sensitivity, accuracy and systematic effects that set the limit on measurement accuracy.

A schematic of the testbed is shown below in Figures 10 and 11. The coronagraph of choice for this setup was the apodized-pupil Lyot coronagraph asit will be used for the starlight suppression system for the Gemini Planet Imager Project. The source optics are shown in the upper-center and left side of the drawing. The testbed instrument itself is shown in the lower right. The testbed is now fully assembled and aligned, and we are getting some preliminary measurements from the coronagraph, the HOWFS and the LOWFS.
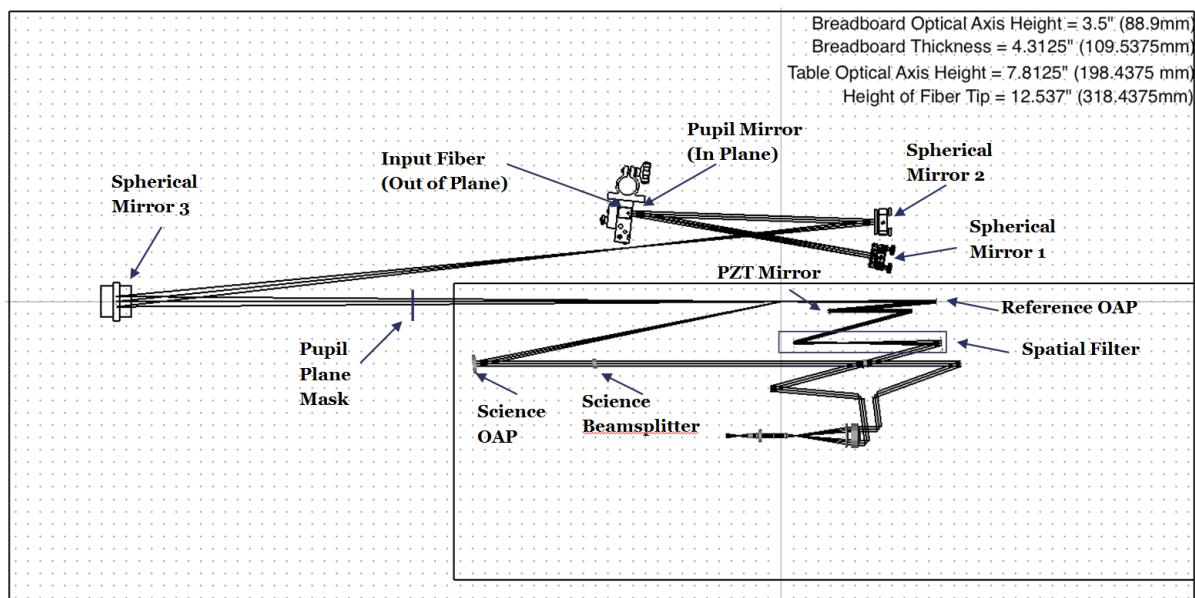
Fig. 4. Layout of the calibration testbed. The source optics are shown in the upper-center and left side of the drawing. The cal instrument itself is shown in the lower right. The cal testbed instrument is a duplicate of the optical system that will be used on Gemini.
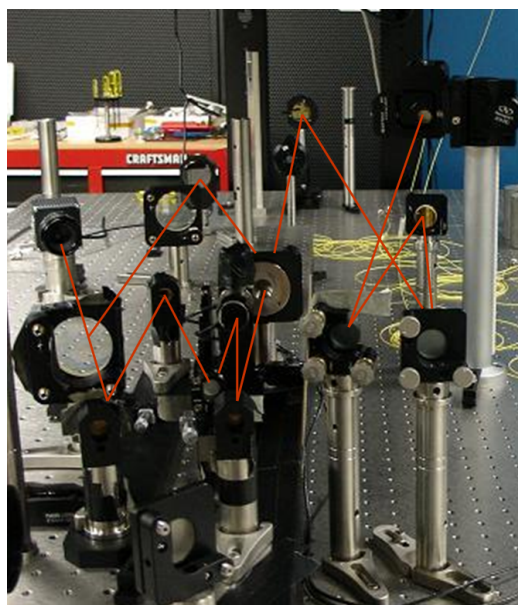

Fig. 5. Photograph of the cal testbed. The red line traces the path of the science arm, and the blue line traces the reference arm of the HOWFS interferometer. The camera in the lower center is the HOWFS camera.

2.1 Cal LOWFS Testbed Results

The current status of the LOWFS wavefront sensor is shown below in Figure 12. The hardware is fully assembled and aligned. Indeed, this hardware will be used on the final GPI instrument. We have a functioning reconstructor and have demonstrated sensing of low order aberrations in the lab. In order to verify the performance of the low order wavefront sensor, we first made a measurement of a wavefront for a glass substrate located in the apodized pupil plane with an infrared Zygo interferometer operating at 1.55 um. This data was then imported into an analysis package, the low-spatial frequencies were extracted, and the data then pixilated to the same resolution as the GPI Cal LOWFS reconstructed

pupil. This spatially filtered Zygo data and the LOWFS reconstruction of the same phase object are shown below in Figure 13.
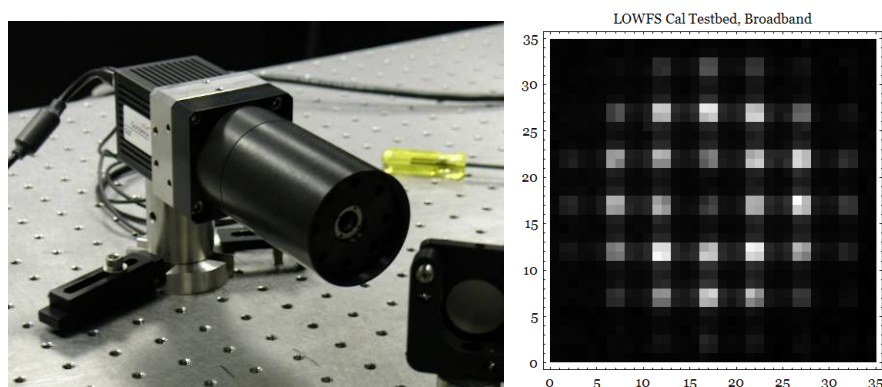

LOWFS Cal Testbed, Broadband

Fig. 6. Low-order wave front sensor results. The Shack-Hartman camera is shown on the left while the image on the right shows the response of the LOWFS pixels. The transmission function of the apodized pupil is clearly evident in the illumination of the 2x2 spots.
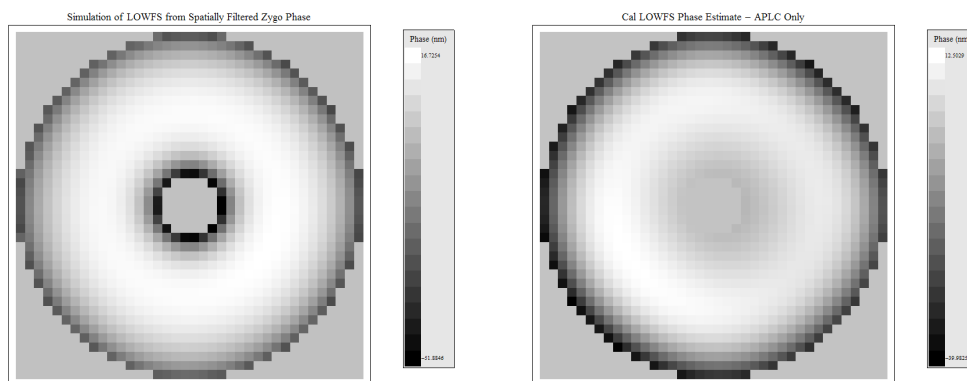

Simulation of LOWFS from Spatially Filtered Zygo Phase

Cal LOWFS Phase Estimate – APLC Only

Fig. 7. Zygo phase measurement compared against LOWFS reconstruction. The measurement on the left is from data taken on a Zygo interfometer operating at 1.55 um. The data has been low passed through the same low pass filter as on the testbed. It was next pixilated to the same sampling as the LOWFS pupil. The LOWFS measurement of the same phase object is on the right. The rms difference between these two data sets was measured to be 7.6 nm, rms.

2.2   Cal HOWFS Testbed Results

The HOWFS data acquisition is done by take a full pupil image as a function of delay. This produces a data cube that is the interference fringe signal per pixel in the pupil. Reconstruction is done by fitting a white light fringe to each pixel in the HOWFS pupil. This fit function is that of a white light fringe packet. The fit parameters are: mean offset, slope of offset, envelope center, fringe envelope width, Sin and Cos component visibilities (Sine and Cosine measured relative to the fringe envelope center). All of these fit parameters contain useful information, however our main interest is in the Sine and Cosine coefficients as these parameters are directly related to the phase and amplitude errors in the apodized pupil plane before the focal plane mask. Figure 14 below shows an example of the raw data and overlaid on top are the fit parameters for that particular pixel in the pupil.

We verified the performance of the HOWFS in a manner similar to that of the LOWFS. We first acquired a static phase perturbation plate that is used in transmission. (For our purposes, this was a microscope slide). This phase perturbation plate was measured with a phase shifting Zygo interferometer working at 633 nm. This raw Zygo data was then processed in the following way: 1) it was spatially filtered to remove phase content below the bandwidth set by the focal plane mask, 2) it was re-sampled to match the pixel pitch of the Cal HOWFS detector. This data then had to be

compared to the HOWFS reconstruction mentioned above. This comparison was laborious as it required fine adjustment of the translation, scale and rotation of the one data set with respect to the other. Figure 15 shows the comparison between the processed Zygo data and the Cal HOWFS reconstruction. Visually, the agreement is already evident. Figure 16 shows the different of these two pupil measurements. The difference was measured to be 4.97 nm rms.
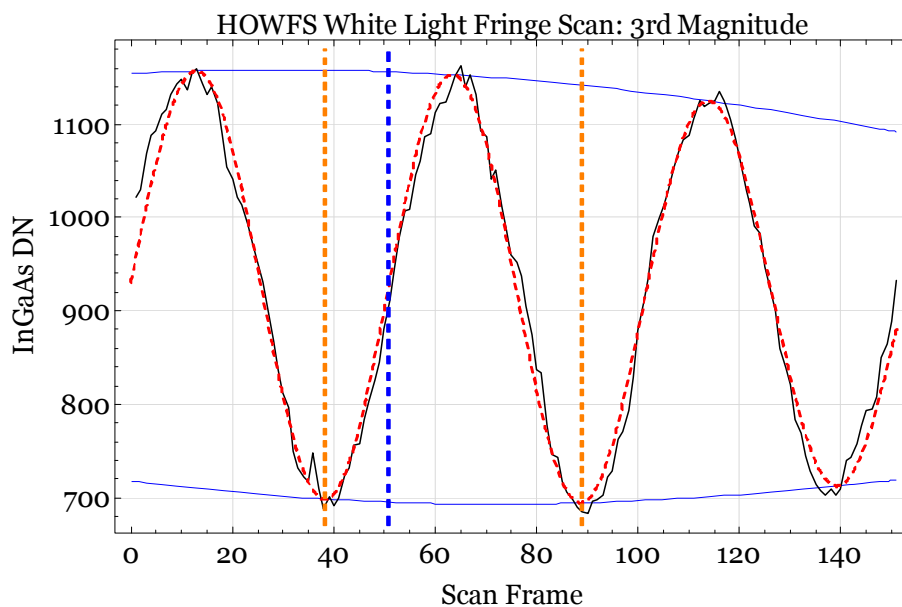

Fig. 8. White light fringe scan on the Cal HOWFS detector. This data set shows the white light scan and the fit parameters: mean offset and offset gradient, envelope center and width, Sine and Cosine coefficients of the fringe visibility, and fringe frequency.
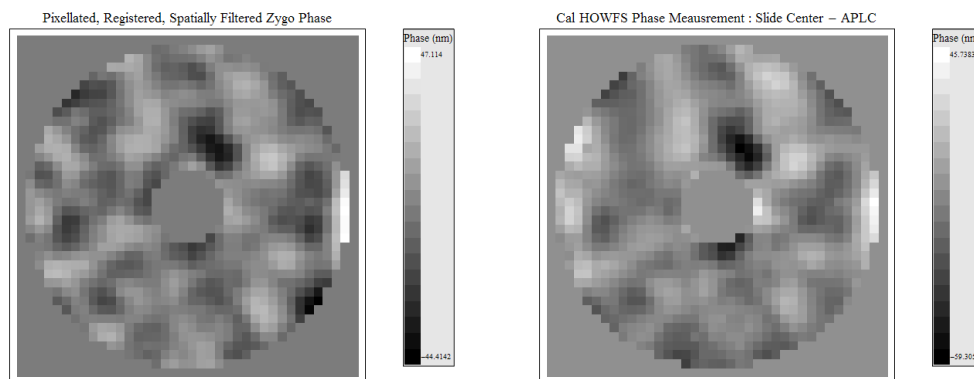

Fig. 9. Validation of the HOWFS measurement using Zygo phase measurement of a phase perturbation plate. The data on the left is derived from data taken with a Zygo working at 633 nm. The raw data has been spatially filtered, pixilated and registered with respect to the HOWFS data. The HOWFS data on the right is simply the map of fit coefficients for the Sine term of the white light fringe for each pixel in the pupil. This data was taken at an equivalent source brightness of 3rd magnitude.
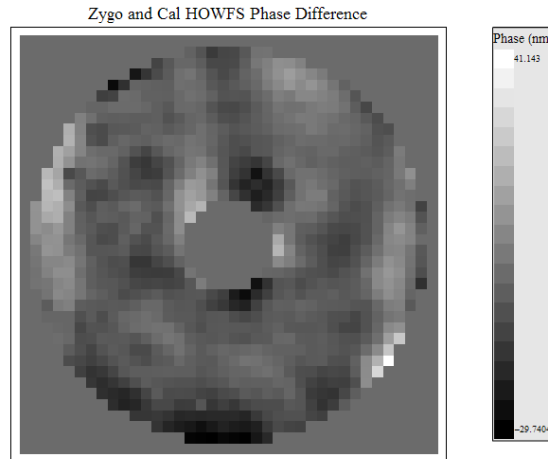
Fig. 10. The difference image between the Zygo data and the Cal HOWFS for pupil phase measurements shown in Figure 9. The difference between the two measurements is measured to be 4.97 nm, rms.

3. CONCLUSION

Testbed results for the GPI calibration system have been described. The validation measurements made by both the LOWFS and the HOWFS met the testbed requirements of 10 nm, rms and 5 nm, rms respectively. These requirements are traceable to those needed for the GPI system and provide re-assuring evidence that the system will work as expected.

4. ACKNOWLEDGEMENTS

REFERENCES

[1] Bruce Macintosh, et. al., "The Gemini Planet Imager: from science to design to construction", Proc SPIE, Vol. 7015, 18, (2008).

[2] S. Shaklan and J.J. Green, "Low-order Aberration Sensitivity of eighth-order coronagraphic masks", ApJ, 628, 474-477 (2005).

[3] R. Soummer, C. Aime, and P.E. Falloon, , "Stellar coronagraph with prolate apodization", A&A 397, 1161-1171 (2003).

[4] Matthew C. Britton, "Arroyo", Proc. SPIE, Integrated Modeling of Extremely Large Telescopes, Vol. 5497, 290 (2004)